Journal of Power Sources 196 (2011) 550–558

Contents lists available at ScienceDirect

Journal of Power Sources

journal homepage: www.elsevier.com/locate/jpowsour

Preparation of mesoporous carbons from amphiphilic carbonaceous material for high-performance electric double-layer capacitors

Jin Wang, Mingming Chen*, Chengyang Wang, Jiuzhou Wang, Jiaming Zheng

Key Laboratory for Green Chemical Technology of Ministry of Education, School of Chemical Engineering and Technology, Tianjin University, Tianjin 300072, PR China

ARTICLE INFO

Article history:
Received 29 April 2010
Received in revised form 9 July 2010
Accepted 13 July 2010
Available online 18 July 2010

Keywords:
Amphiphilic carbonaceous material
Activated carbon
Mesopore
Electric double-layer capacitor

ABSTRACT

Amphiphilic carbonaceous material (ACM), with nanoscale dispersion in alkaline aqueous solutions, is synthesized from green needle coke. As a special precursor with small particle size, plenty of functional groups and widened d_{002} simultaneously, ACM guarantees subsequent ACM-based activated carbons (AACs) with high specific surface area over 3000 $m^2\,g^{-1}$ as well as well-developed mesoporous structure after KOH activation. Such pore properties enable AACs' high performances as electrode materials for electric double-layer capacitors (EDLCs). In particular, surface area up to 3347 $m^2\,g^{-1}$ together with notable mesopore proportion (26.9%) gives sample AAC814 outstanding EDLC behaviors during a series of electrochemical tests including galvanostatic charge/discharge, CV and electrochemical impedance spectroscopy. The electrode gets satisfactory gravimetric and volumetric specific capacitance at the current density of 50 mA g^{-1}, up to 348 F g^{-1} and 162 F cm^{-3}, respectively. Furthermore, for the mesoporosity, there is only a slight capacitance reduction for AAC814 as the current density reaches 1000 mA g^{-1}, indicating its good rate performance. It is all the ACM's unique characteristics that make AACs a sort of competitive EDLC electrode materials, both in terms of specific capacitance and rate capability.

1. Introduction

Electric double-layer capacitors (EDLCs), using activated carbons (ACs) as electrode materials, have been recognized as one of the efficient storage devices for electric power because of their better rate capability and longer cycle life than that of secondary batteries and higher energy density than that of conventional capacitors [1,2]. At present, activated carbons (ACs) are still electrode materials used most frequently in EDLCs for their low cost, high surface area, availability, and established production technologies [3–5]. It has been proven that electrochemical behaviors of EDLCs are strongly affected not only by specific surface area (S_{BET}) of electrodes, but also by other natures of carbon materials such as pore size distribution, surface functional groups and electronic conductivity [4,5].

Particularly, raw materials and activation methods are two of the most important factors which may influence the final structure of ACs. Coal, petroleum coke (PC), and needle coke (NC), with high carbon content, economic cost, low volatile and ash content, are conventional carbonaceous precursors. As far as we know, ACs with surface area beyond 2000 $m^2\,g^{-1}$ have been prepared from these materials via chemical activation, and such kinds of ACs generally have fairly high capacitance [6–11]. However, there are some limitations for developing ACs with ideal EDLC performances from traditional precursors. The cokes are hard to be activated due to stable micrographitic structure and lack of initial pores [8,11,12]. Meanwhile, suffered from large particle size (usually in micron scale) of raw materials, the diffusion of chemicals from surface to central or vice versa is difficult, and therefore causes an inhomogeneous activation. It is unavoidable that some light components may stay inside the particles and pyrolyze under high temperature, obstructing the microporous networks. Accordingly, a large amount of chemical reagents are needed for activation, which brings many problems, such as excess product cost and environment pollution. Furthermore, ACs obtained from traditional precursors are usually micropore dominant materials. For their micropore scale, the mass transfer resistances for electrolyte ions become stronger at high current densities, leading to unfavorable rate capability [5].

To solve these abovementioned drawbacks, pre-treatment of precursor is a simple and effective way. Voluminous researches have been done on pre-oxidation of carbonaceous raw materials, either by air [13,14] or oxidizing solutions [12,15]. The pre-modifications resulted in more active sites and wider d_{002} of the graphitic microcrystallines for the precursors, which accelerated the disintegration of aromatic structures during activation. But these works majorly focused on surface decoration by functional groups and hardly changed the micron-scale contact of precur-

* Corresponding author. Tel.: +86 22 2789 0481; fax: +86 22 2789 0481.
E-mail address: chmmxu@gmail.com (M. Chen).

0378-7753/$ – see front matter © 2010 Elsevier B.V. All rights reserved.
doi:10.1016/j.jpowsour.2010.07.030

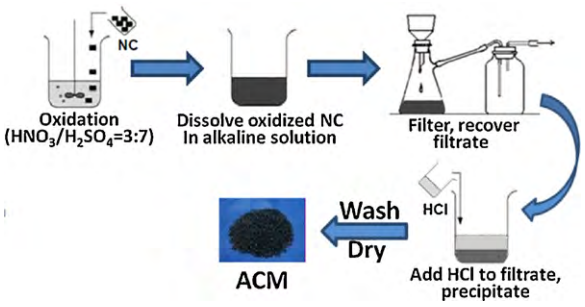

Fig. 1. Schematic flow chart for the ACM preparation.

sor particles with chemical agents. So, although ACs with S_{BET} around 2500 $m^2 g^{-1}$ were obtained under low quantity of chemicals [12,13,15], there still exists potential for improvement. Besides, Gogotsi's group has pointed out that nano-sized electrode materials could exhibit superior properties in EDLCs, including faster kinetics, lower resistance, and improved stability [16]. Unfortunately, these features seem unattainable for ACs from micron-sized precursors. In general, pre-modification methods which can break precursors into nano-pieces should be practicable for further design of high-performance ACs in EDLCs.

It was found that the concentrated nitro-sulfuric acid treatment can forcibly lead to structural change of raw coke. The product, soluble in both alkaline aqueous solutions and polar organic solvents, is called "Amphiphilic carbonaceous material" (ACM) [17]. In previous work [18], it has been found that the links between adjacent graphitic microcrystallines in raw coke were broken during the preparation. Therefore, unlike those pre-oxidized precursors, ACM not only has sufficient surface functional groups and widened d_{002}, but also can disperse in alkaline aqueous solutions in nano-scale [18,19]. Based on its unique properties, ACM is supposed to possess various advantages over traditional precursors during chemical activation. In this work, ACM-based activated carbons (AACs) with nice porous structure were obtained through KOH activation. As expected, the resultant AACs exhibit large specific capacitances as well as nice rate capabilities for EDLCs.

2. Experimental

2.1. Preparation and characterization of samples

Green NC derived from residual oil was provided by Jinzhou Petrochemical Co. in China. The coke was prepared around 500 °C in a delayed coker. ACM was synthesized by oxidation of raw NC with a mixture of concentrated nitric acid and sulfuric acid (v/v = 3/7) and details have been described in earlier reports [17]. A schematic flowchart for ACM preparation is shown in Fig. 1.

AACs were then prepared from ACM by KOH activation. KOH and ACM at different mass ratios (2, 4 or 6) were added into plenty of water and stirred for 1 h at 60 °C. After dried at 110 °C for 8 h, the mixtures were heated to the final activation temperatures (700, 800, or 900 °C) at a rate of 10 °C min^{-1} in a tubular furnace under N_2 atmosphere, and maintained for 0.5, 1 or 2 h. All the semi-products were then repeatedly washed with 1 M HCl solution and distilled water in turn until they were free of chloride ions. Finally, after drying, a series of AACs were obtained. Samples prepared in this manner are named and listed in Table 1.

Table 1
Activation conditions of samples.

AAC samples	Activation time (°C)	Residence time (h)	KOH/ACM (in weight ratio)
AAC812	800	1	2:1
AAC814	800	1	4:1
AAC816	800	1	6:1
AAC714	700	1	4:1
AAC914	900	1	4:1
AAC80.54	800	0.5	4:1
AAC824	800	2	4:1

Table 2
Atomic percentage of various elements on the surface of the samples.

Samples	C (%)	O (%)	N (%)	S (%)
NC	92.4	7.2	0.4	–
ACM	78.2	19.1	2.2	0.5

X-ray photoelectron spectroscopy (XPS) was performed on a PHI-1600 ESCA electron system (America PE Company) with Al Kα (1486.6 eV) X-ray source. Porous structures of AACs were characterized by N_2 adsorption/desorption at 77 K on Micrometrics Tristar 3000. Samples were degassed under high vacuum at 300 °C for 4 h before the measurements. An FEI Tecnai G2 F20 transmission electron microscope (TEM) was further used to observe microcrystalline of AACs.

2.2. Electrochemical measurements

Symmetric capacitors were assembled with polypropylene membrane as separator and 6 M KOH aqueous solution as electrolytes, respectively. The electrodes (13 mm in diameter, around 200 μm in thickness) were obtained by pressing a mixture of AACs series (85 wt%), acetylene black (10 wt%), and polytetrafluoroethylene (5 wt%) to the nickel foam current collector.

Galvanostatic charge/discharge analysis was carried out in an Arbin MSTAT instrument. The specific capacitance of the EDLC was calculated according to the following formula:

$$C = \frac{I\Delta t}{\Delta V X} \quad (1)$$

where C represents for the gravimetric specific capacitance ($F g^{-1}$) or volumetric specific capacitance ($F cm^{-3}$), I for the current (A), Δt for the discharge time period (s) of the potential change ΔV (V), X for the carbon mass (g) in a single electrode or volume (cm^3) of the electrode. Cyclic voltammetry (CV) and electrochemical impedance spectroscopy (EIS) tests were carried out on a PARSTAT 2273 system (Princeton applied research). The potential range of CV was 0–1.0 V at sweep rate 5 mV s^{-1} and the Nyquist plots were recorded at the frequency from 100 kHz to 1 mHz. All electrochemical measurements were carried out at room temperature.

3. Results and discussion

3.1. XPS analysis of ACM

It has been earlier proved by XRD and FTIR results that nitro-sulfuric acid treatment broke the links between adjacent graphitic microcrystallines in cokes and brought in many oxygen-containing functional groups [18,20]. The resultant ACM showed widened d_{002}, and could be dissolved in alkaline aqueous solutions [17–20]. Moreover, to study the activation mechanism of ACM, elemental composition and chemical bonds information are extremely important.

The surface elemental composition of raw NC and ACM were evaluated by XPS, listed in Table 2. The analysis shows that NC is composed mainly by C and some amount of O. Compared with NC, there are significant increases of O, N and S in ACM, with their atomic percentage of 19.2%, 2.2% and 0.5%, respectively. Chemical bonds can be studied from high-resolution C1s XPS spectra of samples. The best fitting is invariably obtained with Gaussian lines. Deconvolution of both C1s spectra gives three peaks representing carbon atoms bonded to carbon and/or hydrogen atoms (Peak 1, BE = 284.6–285.1 eV), carbon atoms in alcohol or ether groups (Peak 2, BE = 286.3–287.0 eV), and carbon atoms in carbonyl or carboxyl group (Peak 3, BE = 287.5–290 eV) [21]. The peak in the 287.4–288.5 eV regions (Peaks 3) also relates to C–N bond resulted from the $–NO_2$ group. Obviously, ACM shows a weaker Peak 1 than raw NC, suggesting a decrease of C–C bonds in this material. Meanwhile, increase of Peak 3 in ACM gives evidence for carboxylation and nitration during preparation.

From XPS tests, it is confirmed that O, N, and S atoms were introduced during nitro-sulfuric acid oxidation, and functional groups such as –COOH, –OH, $–NO_2$ and $–SO_3H$ were formed meantime. These groups are hydrophilic and tend to react with alkalis, thus make ACM dispersible in alkali aqueous solutions. Nevertheless, the graphene sheets are too stable to be broken and small hexag-

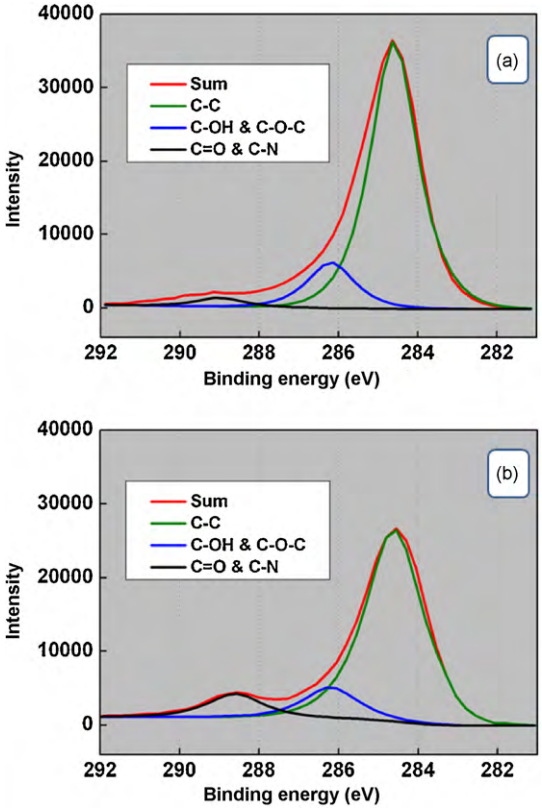

Fig. 2. C1s XPS high-resolution spectra of (a) NC, and (b) ACM.

onal carbon rings are still dominant structure of ACM (Fig. 2b and Table 2), which is the guarantee for high yield of activated products.

3.2. Porous textures of AACs

Pore structure parameters of the AACs were tested by N_2 adsorption/desorption. From Table 3, all these AACs show high S_{BET} (>2000 $m^2\ g^{-1}$), while some of them have over one-fourth mesopore proportion. Among them, AAC814 displays the largest number up to 3347 $m^2\ g^{-1}$ with a mesopore rate of 26.9%. In comparison, according to our previous work [18], activated carbon direct prepared from NC under the same activation condition as AAC814 only had a S_{BET} of 1926 mg^{-1}. Both Yoon's [9] and Li's research groups [11] reported NC-based ACs with comparable S_{BET}, 2900 $m^2\ g^{-1}$, but consumed more KOH (KOH/NC weight ratio 7/1). Researchers in Dalian University of Technology [12,15] pre-modified precursors by $HClO_4$ or H_2O_2, and obtained products with S_{BET} around 2500 mg^{-1} (KOH/precursor weight ratio 4/1). Additionally, the mentioned ACs products [9,11,12,15] are definitely microporous materials.

Such porous properties of these AACs samples are attributed to the characteristics of ACM precursor. First, for the nano-sized dispersion in KOH aqueous solution, every ACM micro-domain has a direct contact with KOH after the mixing. So, the activation was homogeneous and light components generated from gasification also release easily, leading to an efficient activation. Second, the hetero-atoms in ACM are chemically instable and remarkably lower the activation energy of bonded C atom. To some extent, it is these hetero-atoms that provide more "active sites" for activation. Based on Gañan [22] and Lu et al.'s [15] conclusions, the selective reaction of KO with carbon precursors and K intercalation in turbostratic graphitic layers are two key factors for KOH activation. Therefore the diffusion of chemical reagents to the active sites is an important step. Nano-scale contact with KOH, sufficient "active sites" combined with widened d_{002} made pore creating and widening more easily for ACM than traditional precursors.

Of course, besides raw materials, there are many other parameters which affect the porous textures of resulted ACs. To establish the optimum condition for AACs preparation, effects of KOH/ACM ratio, activation temperature, and residence time were further investigated.

3.2.1. Effects of the KOH/ACM ratio

The influences of different KOH/ACM weight ratios were studied with fixed activation temperature (800 °C) and residence time (1 h). Obviously, the shape of N_2 adsorption/desorption isotherms for these AACs are different (Fig. 3a). The isotherms for AAC812 are of particular type I with a well-defined plateau, characteristic of its microporous feature. On the contrary, AAC814 and AAC816 have N_2 adsorption/desorption isotherms of type IV, suggesting the presence of mesopores. Pore size distributions of the three ACs are shown in Fig. 3b for further understanding of the developed porous structure. Increase of the KOH/ACM weight ratio can enlarge the pore size of AACs. For AAC812, most of the pores belong to micropores (diameter <2 nm), while there are certain amounts of small mesopores (diameter 2–5 nm) in AAC814 and AAC816.

The reagent/precursor ratio is the most important parameter in a chemical activation. It is reported that there are usually three stages in the pore development during activation: (1) opening of previously inaccessible pores; (2) creating of new pores by selective activation; (3) widening of the existing pores [23]. Stages (1) and (2) contribute to the micropore formation, which start at the beginning of activation. Step (3), pore widening caused by reaction inside the opened pores, normally takes place after stages (1) and (2), especially under high chemical agent/precursor ratio. To some extent, the pore structure of resultant AC can be adjusted by changing the proportion of steps (1), (2) and (3) in chemical activation. For AAC812, a lower KOH/ACM weight ratio 2/1 made the reaction stop at step (1) or (2), resulting in microporous ACs with lower S_{BET}. If the ratio was raised up to 4/1, the reagent began to be enough for pore creation, and stage (3) also took place under this circumstance. As

Table 3
Porosity parameters of AACs.

Samples	S_{BET}[a] ($m^2\ g^{-1}$)	S_{mic}[b] ($m^2\ g^{-1}$)	S_{mes}[c] ($m^2\ g^{-1}$)	S_{mes}/S_{BET} (%)	V_{tot}[d] ($cm^3\ g^{-1}$)
AAC812	2256	2153	103	4.6	1.0
AAC814	3347	2446	901	26.9	1.8
AAC816	2765	1887	878	31.8	2.4
AAC714	2630	2500	130	4.9	1.4
AAC914	2829	2021	808	28.6	2.3
AAC805.4	2552	2384	168	6.6	1.2
AAC824	3033	2182	851	28.0	2.0

[a] Specific surface area from multiple BET method.
[b] Micropore surface area from *t*-plot method.
[c] Mesopore surface area.
[d] Total pore volume at $p/p_0 = 0.99$.

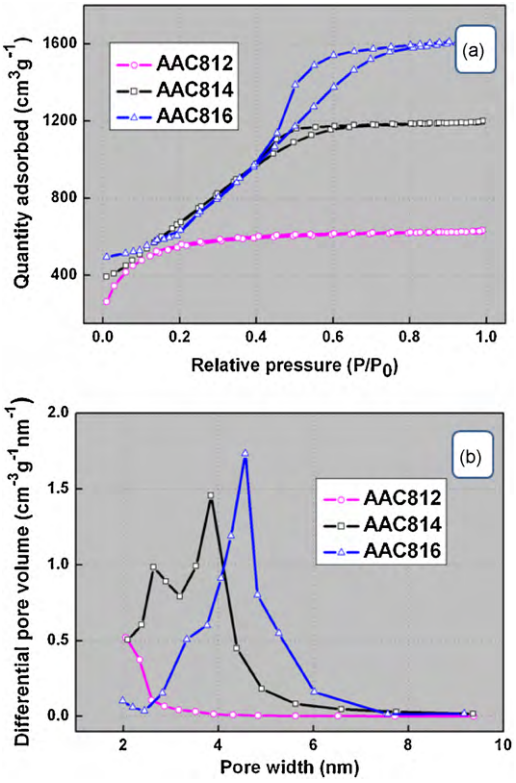

Fig. 3. (a) N2 adsorption isotherms and (b) pore size distributions of AACs with different KOH/ACM weight ratio.

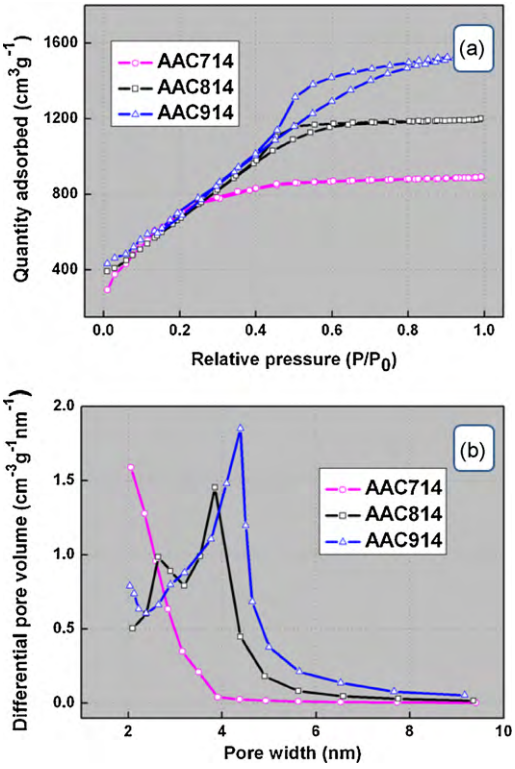

Fig. 4. (a) N2 adsorption isotherms and (b) pore size distributions of AACs with different activation temperature.

a result, AAC814 got a high S_{BET} up to 3347 $m^2\ g^{-1}$ combined with well-developed mesoporous structure. As the increase of KOH concentration, pore widening rather than pore creating would take the domination in reaction. Unsurprisingly, for AAC816, excessive KOH caused an increase in V_{tot} and pore size, of course, decrease in S_{BET} (Table 3).

3.2.2. *Effects of the activation temperature*

Fig. 4 exhibits N_2 adsorption isotherms and pore size distributions of AACs prepared under different activation temperature (KOH/ACM ratio was kept at 4 and residence time at 1 h). With the increase of activation temperature, the AACs transform from microporous (AAC714) to mesopore-contained (AAC814 and AAC914) materials. From thermodynamics, temperature is a driving force for chemical reaction. Consequently, suitable activation temperature is necessary for the development of the carbon's porosity and surface area. Activation at 700 °C produced a microporous carbon with lower S_{BET}. Oppositely, higher temperature (800 and 900 °C) forced the reaction between KOH and ACM more vigorously, which enhanced the pore creation and enlargement. However, the over high temperature of 900 °C led to the decrease of S_{BET}. This could be attributed to the collapse and destruction of pores caused by severe thermal treatment and extensive reaction. Comparatively, 800 °C is the critical and favorable temperature, providing interested porous textures to AAC814 (Table 3).

3.2.3. *Effects of the residence time*

To study the effects of activation time on the porous properties of AACs, activations were carried out under different holding time with KOH/ACM weight ratio 4/1 at 800 °C. From results in Table 3 and Fig. 5, it was difficult to obtain a well-developed porosity with short residence time (AAC80.54). For AAC824, a 2 h activation time somewhat decreased the surface area (3033 $m^2\ g^{-1}$) because of excess heat treatment and activation. Meanwhile, it is worth noting

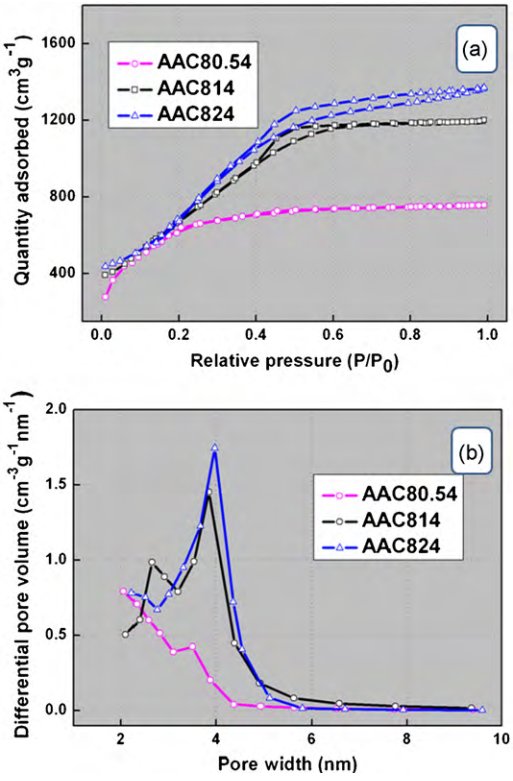

Fig. 5. (a) N2 adsorption isotherms and (b) pore size distributions of AACs with different residence time.

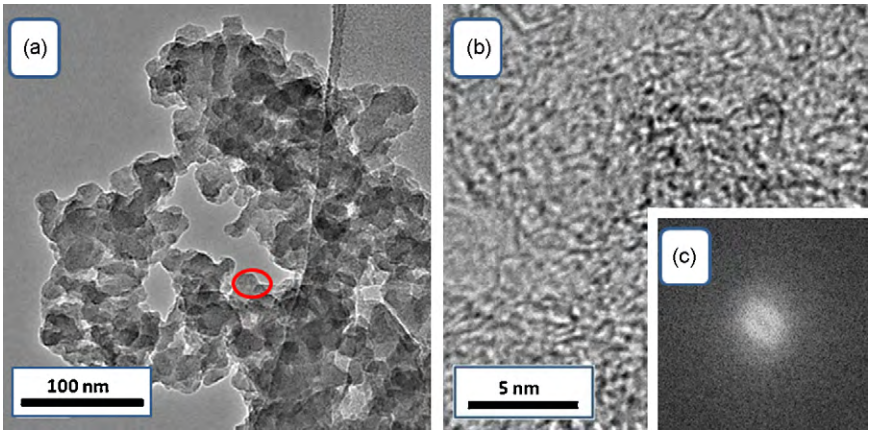

Fig. 6. (a) TEM images of AAC814 particles, (b) high-resolution micrograph of sample, and the inset (c) is the power spectrum of (b).

that residence time has less influence on pore development than KOH/ACM ratio and temperature. The result means that under the given condition (800 °C and KOH/ACM ratio 4/1), selective reaction between KOH and ACM should get close to equilibrium as reaction time above 1 h.

3.2.4. TEM observation of AAC814

As discussed above, the preparation condition for AAC814 is optimum for producing AACs with both high surface area and reasonably mesopore content. Then, TEM was used for further research on the porous texture of this material, detailed in Fig. 6. Apparently, AAC814 consists of small particles in size of 30–50 nm (Fig. 6a). These particles connect to each other and form an aggregate in irregular shapes. Such particle size, as what is predicted from ACM's size, can hardly be obtained from micron-sized precursors. High-resolution micrograph is shown in Fig. 6b. It is noticed that the structure of AAC814 is turbostratic. The bright sections represent pores in the material which are formed by the disordered packing of carbon nano-sheets and clusters. Two-dimensional fast Fourier transform (FFT) power spectrum of the TEM image is displayed in Fig. 6c. The power spectrum indicates the spatial frequency distribution, as the central and surrounding area corresponding to lower and higher frequency, respectively [24,25]. Concentric circles of power spectrum evince the random orientation pore structures for AAC814.

Masking step and inverse fast Fourier transform (IFFT) were taken place on the power spectrum to analyze the pores in more detail. As shown in Figs. 7 and 8, the specific frequency regions in reciprocal space were chosen by ring-shaped mask patterns. After IFFT, images corresponding to pore size 1–2 and 2–5 nm could be obtained. The real space images were then transformed to binary pictures to observe the pore shapes more clearly. Researchers from Tsinghua University [24] proved that the binary image corresponds to the cross section of sliced pores in samples in any arbitrary direction. From the transformed images, both micropore (Fig. 7c) and mesopore (Fig. 8c) exist in AAC814 simultaneously. These irregular pores consist of nano-channels which are connected to and overlap with one another. It is well known that absorption performances of ACs are intimately related to their porous properties. Micropores majorly contribute to high surface area of AAC814, while interconnected mesopores act as mass transfer channels with low intraparticle resistance. Due to the particular pore properties abovementioned, AAC814 could give a nice absorption and transfer capability.

3.3. Electrochemical measurements

Fig. 9a shows the typical charge/discharge curves of AACs electrodes at current density of 50 mA g^{-1}, covering the voltage cope from 0 to 1.0 V. The linear curves are evidences for the ideal EDLC behaviors of all the samples. Obviously, electrode materials with higher S_{BET} show longer charging/discharging time, expressing their larger specific capacitance. Just as what is shown in Fig. 9b, there is a general trend of capacitance increase along with S_{BET}. This is because the energy storage for EDLC is mainly based on accumulation of charge in the double layers formed at the electrode/electrolyte interfaces. Consequently, specific capacity of EDLC largely depends on the surface area of electrode material. For

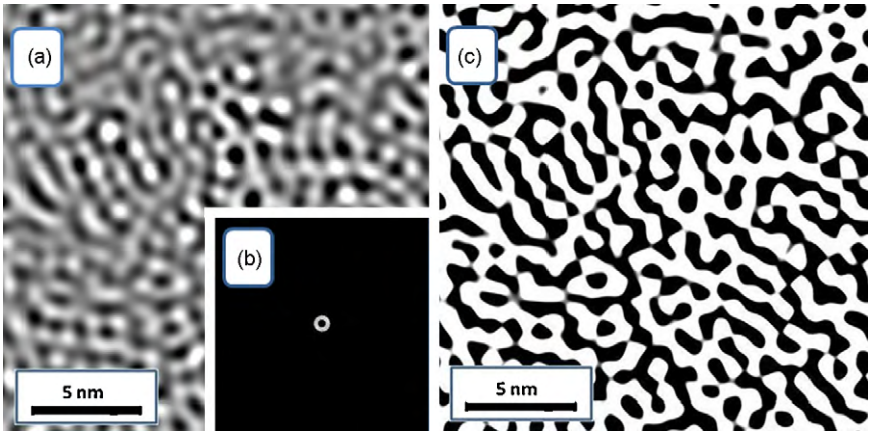

Fig. 7. (a) IFFT image of AAC814 after filtering of the power spectrum in Fig. 6b, inset (b) is the filter pattern corresponding to pore size 1–2 nm and (c) is binary image of (a).

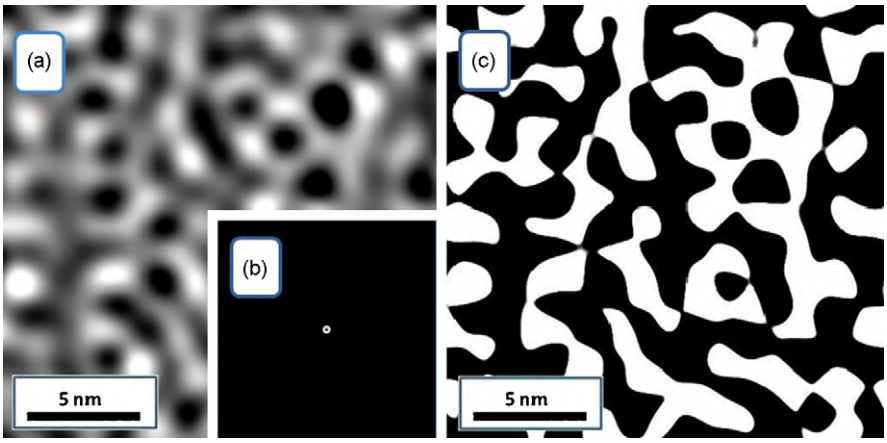

Fig. 8. (a) IFFT image of AAC814 after filtering of the power spectrum in Fig. 6b, inset (b) is the filter pattern corresponding to pore size 2–5 nm and (c) is binary image of (a).

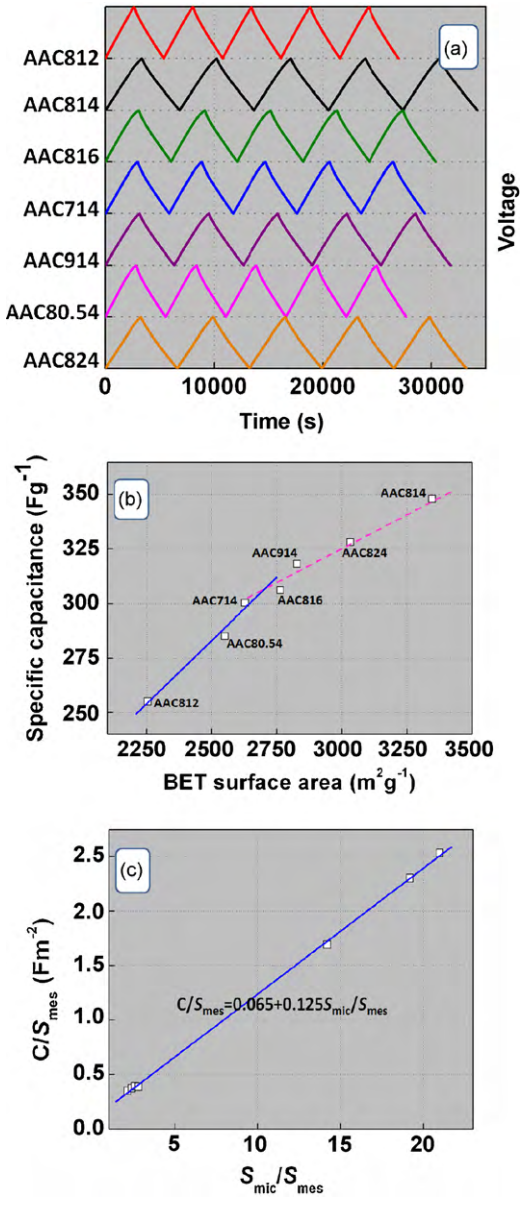

Fig. 9. (a) Charge/discharge performances of AACs electrodes at current density of 50 mA g^{-1}, (b) linear relationship between capacitance and S_{BET} of AACs electrodes, and (c) C/S_{mes} plots as a function of S_{mic}/S_{mes} for all the samples (The solid line is the least square fit to data).

example, the S_{BET} of AAC814 is 3347 m^2 g^{-1}, thus gives this sample highest gravimetric specific capacitance up to 348 F g^{-1}. Such capacitance can hardly be obtained from ACs produced direct from NC [11,18].

According to their pore structure, AACs were divided into two groups, micropore group (AAC812, AAC714, and AAC80.54) and mesopore group (AAC814, AAC816, AAC914, and AAC824). Both groups of carbons show a linear relation between capacitance and S_{BET}. However, the slope of the linear line for microporous samples is much higher than that of mesoporous samples, which means the surface area of microporous carbons is more efficiently used in the energy storage. It has been proven that the capacitance contributions by micropores and mesopores are different [26–30]. Gogotsi's group classically expounded that pores in smaller size (less than the solvated ion size) showed larger normalized capacitance than mesopores [30]. Shi suggested that specific capacitance from galvanostatic charge/discharge and specific surface area from gas sorption technique are sufficient to help distinguish the capacitance contribution of pores in different sizes [26]. From the methodology adopted by Shi, the total specific capacitance (C) is simply:

$$C = S_{mes}C_{mes} + S_{mic}C_{mic} \quad (2)$$

where C_{mes} and C_{mic} are specific capacitance contributions (μF cm^{-2}) from mesopores and micropores. Then using S_{mic}/S_{mes} for X-axis and C/S_{mes} for Y-axis, a linear equation could be obtained:

$$\frac{C}{S_{mes}} = C_{mes} + C_{mic}\frac{S_{mic}}{S_{mes}} \quad (3)$$

The slope and y-intercept of this line should be C_{mic} and C_{mes}. Following this methodology, a linear relation for AACs samples was obtained, shown in Fig. 9c. It is evident that the data is relatively well fitted to this linear relation. From the linear fit, C_{mic} and C_{mes} were calculated to be 12.5 and 6.5 μF cm^{-2}, respectively. The C_{mic} is in a good agreement with that reported in the literatures before [26,31], while the C_{mes} only one half of C_{mic}. So, it can be directly inferred that the micropores of AACs play an essential role for the accumulation of charges, and contribute more to the total capacitance. This is helpful to realize the phenomenon in Fig. 9b.

Though mesopores have less support on the specific capacitance, their role as ion transfer channels is of great importance for the rate performances of samples. The gravimetric specific capacitances at different current densities are listed in Fig. 10a to help estimating the rate properties. For all the samples, capacitances decrease with the rise of current densities. As a microporous material, AAC812 gets a gravimetric specific capacitance of 199 F g^{-1} at the current density 1000 mA g^{-1}, only about 76% of that at 50 mA g^{-1}. The poor capacity maintenances are also found in

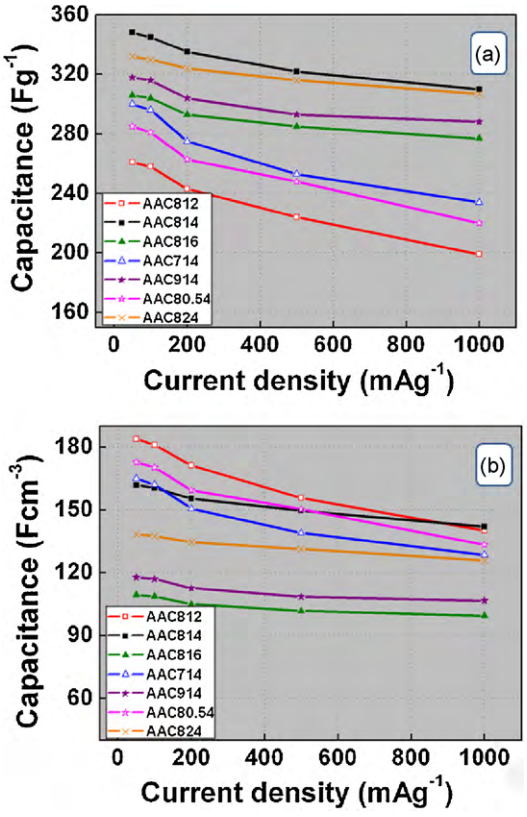

Fig. 10. (a) Gravimetric capacitance and (b) volumetric capacitance of samples at different current densities.

AAC714 (78%), AAC80.54 (79%), and these NC-based ACs mentioned before [9,11,18]. Differently, samples AAC814, AAC816, AAC914 and AAC824 hold about 90% of their capacitance at the high current density, suggesting good rate capability. It has been confirmed that mesopores' size and their interconnectivity strongly influence the dynamic mass transfer properties of the EDLCs. For these mesoporous carbons, the inner-pore ion-transport resistances are significantly lowered by the connected mesopores. This facilitates the electrolyte ion to move quickly at high current densities, and thus gives ideal rate performance to the samples.

Apart from the gravimetric specific capacitance, the volumetric specific capacitance is especially important for commercial application. The volumetric specific capacitances of samples at different current densities are shown in Fig. 10b. As is known to all, high density is often in contradiction with well-developed porous structure. Therefore, it is necessary to balance the porosity and density of samples to optimize the volumetric performances. AAC812, with lowest S_{BET} and V_{tot} of all the samples, gets a volumetric capacitance of 184 F cm^{-3} at current density 50 mA g^{-1}, even better than AAC814 (162 F cm^{-3}). On the contrary, too much pore volume (above 2 cm^3 g^{-1}) results in low electrode density of AAC816 and AAC914, and thus poor volumetric behaviors. However, there are considerable capacitance reductions for these microporous samples at high current densities. Unsurprisingly, profiting from its nice rate capability, AAC814 maintains its volumetric capacitance as high as 142 F cm^{-3} at the current density 1000 mA g^{-1}. This number is higher than those of microporous samples (AAC812, AAC714 and AAC80.54) under the same test conditions.

To clarify the cycling stability of AACs, all the samples endured 900 cycles charge/discharge, with a current density of 50 mA g^{-1} and voltage from 0 to 1.0 V. The values of specific capacitance as a function of cycle number are given in Fig. 11. All the samples maintain their capacity fairly well over time, indicating their

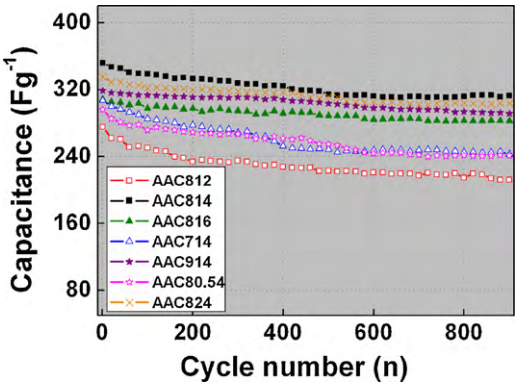

Fig. 11. Specific discharge capacitance as a function of cycle number for the EDLCs (current density 50 mA g^{-1}).

high electrochemical reproducibility as well as good interfacial contact after long-term charge/discharge. The slight capacitance drops at the beginning should be related to some irreversible reactions caused by the trace residual functional groups in AACs. As discussed in Section 3.2, AAC814, AAC816, AAC914, and AAC824 were prepared from intensive reaction with KOH, which consumed most of functional groups in precursor. Therefore, these four samples performed more stably in KOH electrolyte during repeatedly charge/discharge, and their final capacity retentions are 90.4%, 92.5%, 92.1%, and 92.4%, respectively.

CV measurement was further employed to monitor the electrochemical behaviors of the electrodes. From Fig. 12, CV curves obtained at voltage scan rate of 5 mV s^{-1} are nearly rectangular, especially for samples with high mesopore proportion (AAC814, AAC816, AAC914 and AAC824). There is no evidence for any redox currents on both positive and negative sweeps, and currents are almost constant over most of the potential range. As expected, samples with higher specific capacitance show larger area of CV curves. Overall, these AACs electrodes are highly capacitive and electrochemical reversible, with good stability in the alkaline KOH electrolyte.

By the comparison of capacitance, rate capability, and electrochemical stability of AACs samples, AAC814 electrode shows outstanding EDLC performances than others. However, the effects of the mesopores/micropore ratio on complete EDLC performances, including charge/discharge kinetics, could not be revealed by galvanostatic charge/discharge techniques alone [29]. EIS tests were then carried out to study the effects of frequency on the AAC814 electrode in detail, and typical Nyquist diagram is given in Fig. 13a. The semicircle in the high frequency region is correlated with the resistance of the electrode itself and the contact resistance between

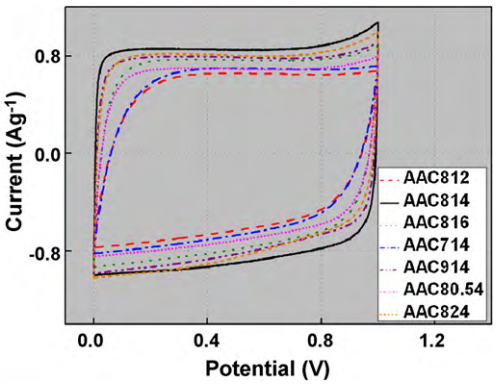

Fig. 12. CV curves of AACs electrodes obtained at scan rate of 5 mV s^{-1}.

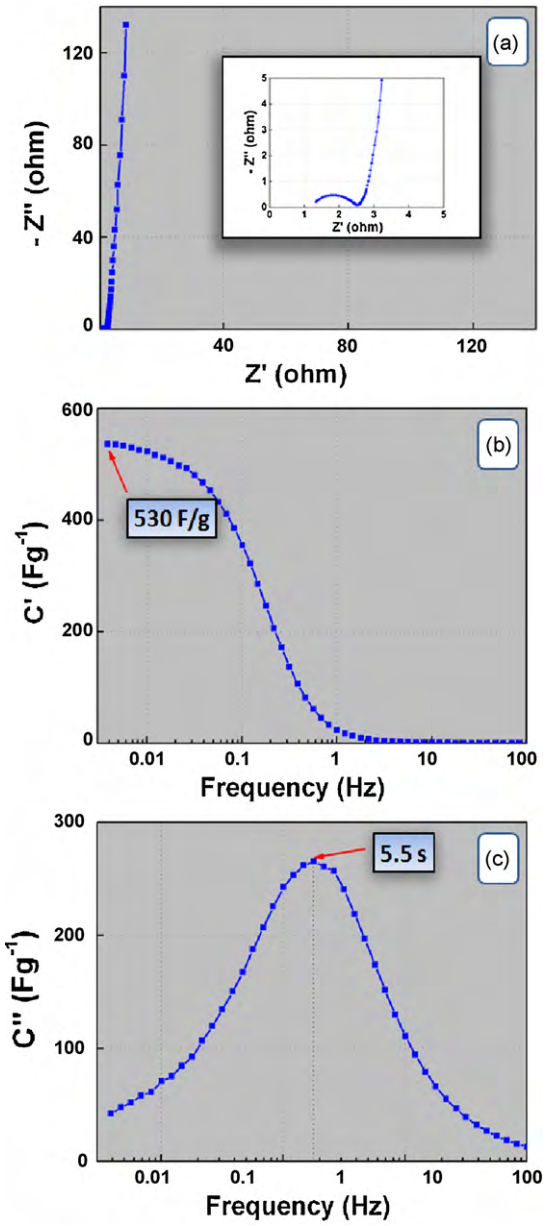

Fig. 13. (a) Nyquist plots for AAC814 electrode with enlarged section of high frequency region in the inset, its Bode plots for real part (b) and imaginary part (c) of capacitance as functions of frequency.

electrode and current collector. For AAC814, nano-scaled particle size brings in a well electrical contact between particles throughout the electrode. Hence, the resistance in this region is only about 1.3 Ω. At low frequency, the imaginary part sharply increases and a nearly vertical line is observed, suggesting the pure capacitive behavior of the electrode.

Bode plots, the real ($C'(\omega)$) and imaginary part ($C''(\omega)$) of the complex capacitance ($C(\omega)$) as a function of frequency, are useful for gaining insight into the electrochemical properties of EDLCs [32]. Fig. 13b presents Bode plots for real part of capacitance ($C'(\omega)$). At the low frequency of 1 mHz, AAC814 shows relatively high capacitance up to 530 F g^{-1}. With the increase of frequency, the capacitance exhibits a frequency dependency, and $C'(\omega)$ drops sharply in the region of 0.01 and 1 Hz. At high frequency, the capacitance is insignificant and the EDLC behaves like a pure resistance. The imaginary part of capacitance ($C''(\omega)$) changes versus frequency is demonstrated in Fig. 13c. The maximum of the curve is a characteristic of the entire system and can be roughly described as the point where the circuit goes from purely resistive to purely capacitive [29]. Relaxation time constant (τ_0), a quantitative measure of how fast the device can be charged and discharged reversibly, is only 5.5 s for AAC814. It is the mesoporosity and small particle size decrease the ion transfer resistance and distance, respectively, and thus give this sample the superior power output ability.

4. Conclusions

AACs with high surface area and small particle size were prepared from ACM by KOH activation. Control and adjustment of their porous parameters were achieved by adjusting activation conditions such as KOH/ACM weight ratio, activation temperature and residence time. Profiting from the ACM precursor with small particle size, plenty of functional group and widened d_{002}, the AACs got high S_{BET} over 3000 m^2 g^{-1} as well as well-developed mesoporous structure under relatively low KOH consumptions.

In electrochemical measurements, the AACs electrodes present nice EDLC behaviors, and there is a general trend of specific capacitance increase along with S_{BET}. The capacitance contribution by micro- and mesopores are different. Micropores play an essential role for the accumulation of charges, while mesopores provide low resistance inner-transfer channels for the electrolyte ions. For owning their optimal mutual ratio, sample AAC814 electrode gets the gravimetric specific capacitance up to 348 F g^{-1} and volumetric specific capacitance 162 F cm^{-3}, at the current density of 50 mA g^{-1}. Even when the current density was raised up to 1000 mA g^{-1}, the two kinds of capacitances are still as high as 300 F g^{-1} and 142 F cm^{-3}, respectively. Moreover, the 900 cycles tests show that these AACs electrodes are stable in KOH electrolyte after long-term charge/discharge. In conclusion, it is precursor's nanosize and other special characteristics that make AACs a sort of competitive electrode materials for EDLCs, both in terms of specific capacitance and rate capability.

Acknowledgements

This work was financially supported by Key Project of Natural Science Foundation of Tianjin City (No. 08JCZDJC17000) and Research Encouragement foundation of Tianjin University.

References

[1] X. Zhang, L. Ji, S. Zhang, W. Yang, J. Power Sources 173 (2007) 1017–1023.
[2] S. Zhao, C.Y. Wang, M.M. Chen, J. Wang, Z.Q. Shi, J. Phys. Chem. Solids 70 (2009) 1256–1260.
[3] Y. Zhu, H. Hu, W.C. Li, X. Zhang, J. Power Sources 162 (2006) 738–742.
[4] Y. Wen, G. Cao, Y. Yang, J. Power Sources 148 (2005) 121–128.
[5] B. Xu, F. Wu, R. Chen, G. Cao, S. Chen, Y. Yang, J. Power Sources 195 (2010) 2118–2124.
[6] M.J. Illan-Gomez, A. Garcia-Garcia, C. Salinas-Martinez de Lecea, A. Linares-Solano, Energy Fuels 10 (1996) 1108–1114.
[7] T. Kawano, M. Kubota, M.S. Onyango, F. Watanabe, H. Matsuda, Appl. Therm. Eng. 28 (2008) 865–871.
[8] S. Mitani, S.I. Lee, S.H. Yoon, Y. Korai, I. Mochida, J. Power Sources 133 (2004) 298–301.
[9] W. Qiao, S.H. Yoon, I. Mochida, Energy Fuels 20 (2006) 1680–1684.
[10] S. Mitani, S.I. Lee, K. Saito, S.H. Yoon, Y. Korai, I. Mochida, Carbon 43 (2005) 2960–2967.
[11] Q. Li, K.X. Li, F.R. Wang, G.H. Sun, New Carbon Mater. 20 (2005) 335–342.
[12] B. Jiang, Y. Zhang, J. Zhou, K. Zhang, S. Chen, Fuel 87 (2008) 1844–1848.
[13] W. Xing, Z.F. Yan, New Carbon Mater. 17 (2002) 25–30.
[14] J.B. Parra, J.J. Pis, J.C. De Sousa, J.A. Pajares, R.C. Bansal, Carbon 34 (1996) 783–787.
[15] C. Lu, S. Xu, M. Wang, L. Wei, S. Liu, C. Liu, Carbon 45 (2007) 206–209.
[16] C. Portet, G. Yushin, Y. Gogotsi, J. Electrochem. Soc. 155 (2008) A531–A536.
[17] D. Tateishi, K. Esumi, H. Honda, H. Oda, Carbon 30 (1992) 942–944.
[18] J. Wang, M.M. Chen, C.Y. Wang, J.M. Zheng, Mesoporous activated carbon from amphiphilic carbonaceous material and its application in EDLC, in: 3rd IEEE INEC, 2010, pp. 222–223.
[19] Z. Li, W. Yan, S. Dai, Carbon 42 (2004) 767–770.

[20] D. Tateishi, K. Esumi, H. Honda, Carbon 29 (1991) 1296–1298.
[21] S. Biniak, G. Szymanski, J. Siedlewski, A. Swiatkowski, Carbon 35 (1997) 1799–1810.
[22] J. Gañan, C.M. González-García, J.F. González, E. Sabio, A. Macías-García, M.A. Díaz-Díez, Appl. Surf. Sci. 238 (2004) 347–354.
[23] F. Rodríguez-Reinoso, M. Molina-Sabio, M.T. González, Carbon 33 (1995) 15–23.
[24] Z.H. Huang, F. Kang, W.L. Huang, J.B. Yang, K.M. Liang, M.L. Cui, Z. Cheng, J. Colloid Interface Sci. 249 (2002) 453–457.
[25] K. Oshida, K. Kogiso, K. Matsubayashi, K. Takeuchi, S. Kobayashi, M. Endo, M.S. Dresselhaus, G. Dresselhaus, J. Mater. Res. 10 (1995) 2507–2517.
[26] H. Shi, Electrochim. Acta 41 (1996) 1633–1639.
[27] C. Largeot, C. Portet, J. Chmiola, P.-L. Taberna, Y. Gogotsi, P. Simon, J. Am. Chem. Soc. 130 (2008) 2730–2731.
[28] R. Lin, P.L. Taberna, J. Chmiola, D. Guay, Y. Gogotsi, P. Simon, J. Electrochem. Soc. 156 (2009) A7–A12.
[29] J. Chmiola, G. Yushin, R. Dash, Y. Gogotsi, J. Power Sources 158 (2006) 765–772.
[30] J. Chmiola, G. Yushin, Y. Gogotsi, C. Portet, P. Simon, P.L. Taberna, Science 313 (2006) 1760–1763.
[31] C.Y. Wu, P.W. Wu, P. Lin, J. Power Sources 195 (2010) 5122–5129.
[32] P.L. Taberna, P. Simon, J.F. Fauvarque, J. Electrochem. Soc. 150 (2003) A292–A300.